Modern Physics Letters B
Vol. 33, No. 11 (2019) 1950134 (11 pages)

DOI: 10.1142/S0217984919501343

World Scientific
www.worldscientific.com

Spin structure and optical properties of cobalt octaethylporphyrin

Dmitriy S. Chub*, Oleg V. Farberovich† and Alexander V. Soldatov‡
The Smart Materials Research Institute,
Southern Federal University, Rostov-on-Don, Russia
**dschub@sfedu.ru*
†*olegfa@bgu.ac.il*
‡*soldatov@sfedu.ru*

Received 25 December 2017
Accepted 12 February 2019
Published 1 April 2019

In this study, we have developed and used the advanced high-precision numerical techniques to accurately calculate the optical properties and spin structure, and access the details of spin dynamics of the cobalt octaethylporphyrin (CoOEP) in the THz pulse magnetic field. The optical spectra of CoOEP are calculated using first-principles based on the GW approximation. The optical properties, including complex dielectric function, optical reflectivity, extinction coefficient, refractive index and absorption coefficient up to 10 eV, together with the calculated spin structure are considered. The spin structure of CoOEP is described by means of the density of spin transitions within the terahertz range. The study covers both terahertz and visible ranges. On the basis of the obtained optical theoretical spectra and the spin structure of CoOEP, it can be concluded that the applied complex approach provides a detailed and accurate description of the optical properties of cobalt octaethylporphyrin within the whole range of energies.

Keywords: Molecular magnets; cobalt octaethylporphyrins; optical properties; dielectric function; femtosecond time resolution.

1. Introduction

Metalloporphyrins are a highly attractive family of molecules with widely varying properties and potential applications. Porphyrins may serve as components of solar cells,[1] nonlinear optical devices,[2] sensors[3] and catalysts,[4] serve as sensitizers in photodynamic tumor therapy,[5] and as components in nanostructures materials.[6,7] The building of small molecules on the basis of metalloporphyrins is a topic of great interest for a number of reasons. Metalloporphyrins are analogs of hemes, therefore, the knowledge of how dioxygen can be linked to metalloporphyrins is critical for our understanding of life.[8] Several gas sensing systems employing metallated

*Corresponding author.

porphyrins have been reported in the literature. Cobalt porphyrins also show promise as electrocatalysts for oxygen reduction.[9–12]

The possibility to control magnetic momentum in a low-dimensional system holds the promise of a number of applications in spintronics.[13,14] Particularly, the strong possibility to fabricate much denser and faster nanocircuits using single magnetic molecules has created a huge interest both in fundamental and applied research.[14–16] A number of studies in these molecular spintronic systems have already shown several promising properties such as giant magnetoresistance,[17] spin injection,[18] spin filtration,[19,20] spin current switching,[21] negative differential resistance[22] and memory effect.[16]

Small isolated molecules with stable paramagnetic ordering are a perfect ingredient for molecular spintronics as well as spin-caloritronic applications.[14,23] In this regard, transition metal-centered metalloporphyrin having localized $3d$ states is one of the hugely explored systems.[23–28] Recent experimental and theoretical studies have already revealed a number of fascinating electronic and spintronic properties.[7,25–32] One of the major targets in spintronics is to control the spin states of the magnetic material by means of various external influences such as light irradiation,[33] temperature control,[34] molecular adsorption,[23,26] substrate interaction,[25] etc. Recently, various studies have demonstrated an efficient way to manipulate the spin state of a metalloporphyrin by reversibly attaching small gaseous molecules to its metal center.[23,26,35] Generally, in this process, small gaseous molecules have to be adsorbed and thermally desorbed repeatedly to tune the spin state of metalloporphyrins.[23] As a result, the process becomes quite energy-consuming and suitable for practical purpose as the desorption stage generally requires very high temperature.[23,26]

In this study, first we thoroughly investigate the optical properties of cobalt octaethylporphyrin (CoOEP). Then, we calculate the spin structure of CoOEP within the THz domain to explore the photo-induced spin-state manipulation. Finally, we simulate the spin dynamics of CoOEP molecule within the THz pulse magnetic field to find out the potential use of molecular magnets in spintronic devices.

An accurate description of the band structure is a precondition for a reliable prediction of optical properties. Manipulating the Fermi level of the system eventually is known to generate pure spin thermopower without changing the components in spintronic devices.

2. Methods

We used the Drude model to describe THz electron response. In this case, the dielectric permittivity function for CoOEP can presented in the form

$$\epsilon_x(\omega) = \tilde{\epsilon}_x^{\mathrm{Drude}}(\omega) + \tilde{\epsilon}_x^{\mathrm{charge}}(\omega) + \alpha_x^{\mathrm{spin}}(\omega)\,, \tag{1}$$

where $\tilde{\epsilon}_x^{\mathrm{Drude}}(\omega)$ is the Drude dielectric permittivity tensor with components; $\tilde{\epsilon}_x^{\mathrm{charge}}(\omega)$ is the dielectric function related to charge polarization; $\alpha_x^{\mathrm{spin}}(\omega)$ is the polarizability tensor.

The Drude dielectric permittivity is presented as

$$\tilde{\epsilon}_x = \epsilon_b \left[1 - \frac{\omega_p^2(\omega^2 + i\omega\Gamma)}{(\omega^2 + i\omega\Gamma)^2 - \omega^2\omega_c^2} \right], \tag{2}$$

where ω_p is effective plasma frequency, ω_c is cyclotron frequency, ϵ_b is background dielectric permittivity and Γ is a damping constant.

The charge polarization dielectric function is

$$\tilde{\epsilon}_x^{\text{charge}}(\omega) = 4\pi\alpha_x^{\text{charge}}(\omega) + 1\,. \tag{3}$$

The polarizability tensor is written as

$$\alpha_x^{\text{spin}}(\omega) = 2\gamma^2 \sum_{i=1}^{N_i} \sum_{f=1}^{N_f} |H_{\text{eff}}^x H_{if}^{(x)}|^2 \frac{\omega_f - \omega_i}{(\omega_f - \omega_i)^2 - (\omega - i\Gamma)^2}\,. \tag{4}$$

For the THz frequency region, we can write the dielectric response as

$$\epsilon_x(\omega) = \tilde{\epsilon}_x^{\text{Drude}}(\omega) + (4\pi\alpha_x^{\text{charge}}(\omega) + 1) + (4\pi\alpha_x^{\text{spin}}(\omega) + 1)\,. \tag{5}$$

2.1. *Optical properties calculations*

The calculation of the optical response proceeded in two steps:

(1) obtaining structural and ground state electronic properties using density functional theory (DFT) and generalized gradient approximation (GGA),
(2) calculating quasiparticle energies by GW approximation using G_0W_0 implementation in the random phase approximation (RPA).

Within the independent particle approximation (IPA) the charge polarization is given by

$$\alpha_{xz}^{\text{charge}}(\omega) = \frac{e^2}{m_e^2 V\omega^2} \sum_{n,m} \sum_{\mathbf{k}} (f_{n\mathbf{k}} - f_{m\mathbf{k}}) \frac{\langle n\mathbf{k}|\hat{p}^x|m\mathbf{k}\rangle\langle n\mathbf{k}|\hat{p}^z|m\mathbf{k}\rangle}{(\epsilon_{n\mathbf{k}} - \epsilon_{m\mathbf{k}}) - (\omega - i\Gamma)}\,, \tag{6}$$

where $f_{n\mathbf{k}} - f_{m\mathbf{k}}$ denote the Fermi occupation factors for the Bloch states $|n\mathbf{k}\rangle$ and $|m\mathbf{k}\rangle$, $\langle n\mathbf{k}|\hat{p}^z|m\mathbf{k}\rangle$ represent the momentum matrix elements of the system, $\epsilon_{n\mathbf{k}} - \epsilon_{m\mathbf{k}}$ are transition energies between states n and m at the point $\mathbf{k}$, $\omega - i\Gamma$ are the frequency and additional small imaginary part which turns on the electromagnetic field adiabatically.

Finally, all the frequency-dependent optical spectra, such as extinction coefficient $k(\omega)$, refractive index $n(\omega)$ and absorption coefficient $a(\omega)$, can be calculated from the real and imaginary parts:

$$n(\omega) = \left[\frac{\sqrt{\varepsilon_1^2 + \varepsilon_2^2} + \varepsilon_1}{2} \right]^{\frac{1}{2}}, \tag{7}$$

$$k(\omega) = \left[\frac{\sqrt{\varepsilon_1^2 + \varepsilon_2^2} - \varepsilon_1}{2} \right]^{\frac{1}{2}}, \tag{8}$$

$$a(\omega) = \sqrt{2}\omega \left[\frac{\sqrt{\varepsilon_1^2 + \varepsilon_2^2} - \varepsilon_1}{2} \right]^{\frac{1}{2}} . \tag{9}$$

We performed spin-polarized DFT-based calculations as implemented in Vienna *Ab Initio* Simulation Package (VASP).[36] The Perdew–Burke–Ernzerhof (PBE) functional within the GGA was used to include exchange–correlation contributions.[37]

All calculations were based on the projector augmented wave (PAW) method.[38] A cutoff of 420.7 eV was chosen for the plane-wave basis set. For the CoOEP calculation, a supercell containing 85 atoms was employed. We carried out geometry optimization for the system without imposing any symmetry constraints where interatomic forces were relaxed up to 0.05 eV/Å.

˜A-centered $3 \times 3 \times 3$ k-mesh within $\tilde{A}$-centered symmetry-reduced Monkhorst–Pack scheme[39] and Gaussian smearing of 0.02 eV were applied to the Brillouin-zone integrations in total-energy calculations.

The valence electron configuration for cobalt is $3d^8 4s^1$. The optical properties based on dielectric function were calculated using *ab initio* principles within the GW approximation,[40] where the self-energy was expressed in terms of the single-particle Green's function and screened Coulomb interaction. The frequency-dependent dielectric response including local field (LF) effects in the RPA,[41] Gaussian smearing of 0.01 eV and $\tilde{A}$-centered $4 \times 4 \times 4$ k-mesh were applied in the optical studies. To visualize the VASP calculated data, the p4vasp code[42] and Origin Pro 8.1 graphing software[43] were used.

2.2. *Spin density simulation*

In our model, the spin structure of the CoOEP molecule can only be described by the spin model of the molecule. We use the idea of spins as a degree of freedom.[44] The spin structure is

$$\langle \hat{S} \rangle = \sqrt{\langle \hat{S}_x \rangle^2 + \langle \hat{S}_y \rangle^2 + \langle \hat{S}_z \rangle^2} \, . \tag{10}$$

We can obtain the quantum mechanical expectation values:

$$\langle \hat{S}_x \rangle = \langle SM | \hat{S}_x | SM \rangle, \tag{11}$$

$$\langle \hat{S}_y \rangle = \langle SM | \hat{S}_y | SM \rangle \, , \tag{12}$$

$$\langle \hat{S}_z \rangle = \langle SM | \hat{S}_z | SM \rangle \, . \tag{13}$$

With the algebra of the spin operators, we can obtain the expectation values for spin-Hamiltonian:

$$\langle \hat{S}_x \rangle = \frac{1}{2} \sum_{\mu=1}^{N} c_\mu^2 A_\mu \, , \tag{14}$$

$$\langle \hat{S}_y \rangle = \frac{i}{2} \sum_{\mu=1}^{N} c_\mu^2 B_\mu \, , \tag{15}$$

$$\langle \hat{S}_z \rangle = \sum_{\mu=1}^{N} c_\mu^2 M^{(\mu)} \,, \tag{16}$$

where

$$A_\mu = \sqrt{S^{(\mu)}(S^{(\mu)}+1) - M^{(\mu)}(M^{(\mu)}+1)} + \sqrt{S^{(\mu)}(S^{(\mu)}+1) - M^{(\mu)}(M^{(\mu)}-1)} \tag{17}$$

and

$$B_\mu = \sqrt{S^{(\mu)}(S^{(\mu)}+1) - M^{(\mu)}(M^{(\mu)}+1)} - \sqrt{S^{(\mu)}(S^{(\mu)}+1) - M^{(\mu)}(M^{(\mu)}-1)} \,. \tag{18}$$

The spin density can be found by inserting the following functions:

$$S_x = \sum_{\mu=1}^{N} c_\mu^2 A_\mu \delta(\epsilon - \epsilon_\mu) \,, \tag{19}$$

$$S_y = \sum_{\mu=1}^{N} c_\mu^2 B_\mu \delta(\epsilon - \epsilon_\mu) \,, \tag{20}$$

$$S_z = \sum_{\mu=1}^{N} c_\mu^2 M^{(\mu)} \delta(\epsilon - \epsilon_\mu) \,, \tag{21}$$

therefore, the spin density is

$$S(\epsilon) = \sqrt{S_x^2(\epsilon) + S_y^2(\epsilon) + S_z^2(\epsilon)} \,. \tag{22}$$

3. Results and Discussion

Figure 1 shows the calculated band structure and density of states (DOS) for CoOEP.

The molecule of CoOEP is shown in Fig. 2.

The presented results of the conducted theoretical study describe the optical properties, spin structure and spin dynamics of the CoOEP molecule in the terahertz pulsed magnetic field.

The calculated real and imaginary parts of dielectric function are presented in Figs. 3 and 4, respectively. The calculations were performed without the LF effects and including the local field effects in both the RPA approximation and time-dependent DFT (TD-DFT) approximation.

The theoretical optical spectra of extinction coefficient, absorption coefficient and refraction index have been obtained (Figs. 5–7).

The comparison of theoretical absorption spectra of CoOEP molecule with the experimental spectra of CoOEP in toluol (Fig. 8) indicates that there is a feature at 3.8 eV, which is thought to be caused by an interband optical transition.

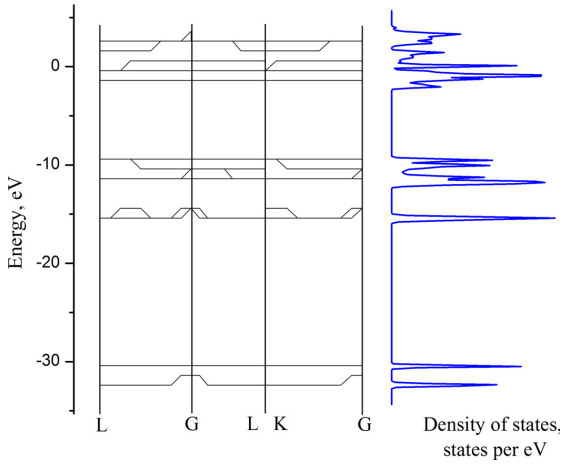

Fig. 1. Band structure and DOS for CoOEP.

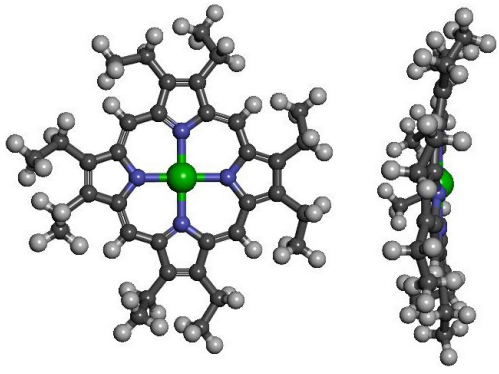

Fig. 2. (Color online) The molecule of CoOEP, in which the Co, N, C and H atoms are represented with green, blue, dark gray and light gray balls, respectively.

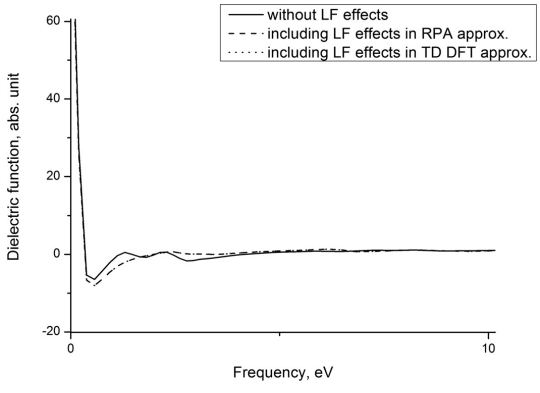

Fig. 3. The calculated real part of dielectric function. The spectra without LF effects and including LF effects in the RPA approximation and TD-DFT approximation are represented with solid, dashed and dotted lines, respectively.

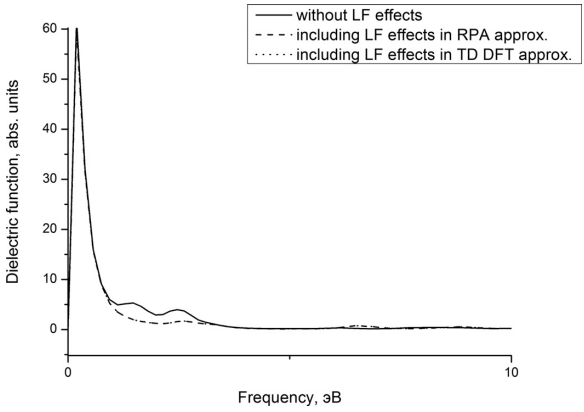

Fig. 4. The imaginary part of dielectric function. The spectra without LF effects and including LF effects in the RPA approximation and TD-DFT approximation are represented with solid, dashed and dotted lines, respectively.

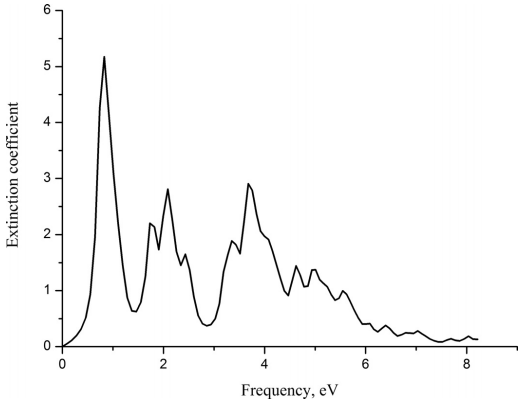

Fig. 5. The calculated extinction spectrum.

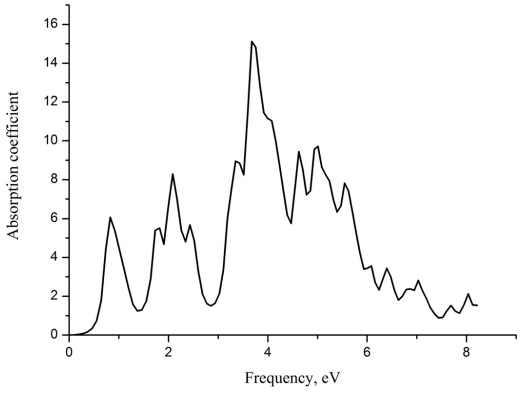

Fig. 6. The calculated absorption spectrum.

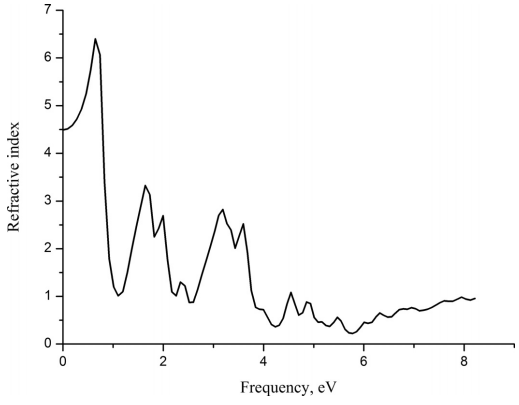

Fig. 7. The calculated refractive spectrum.

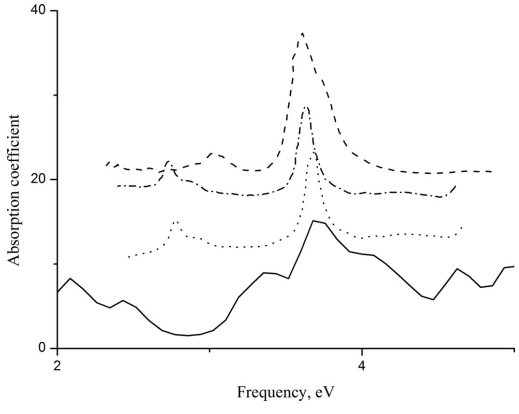

Fig. 8. Comparison of the calculated CoOEP absorption spectrum (solid line) with the experimental spectra of CoOEP in toluol (dashed line).

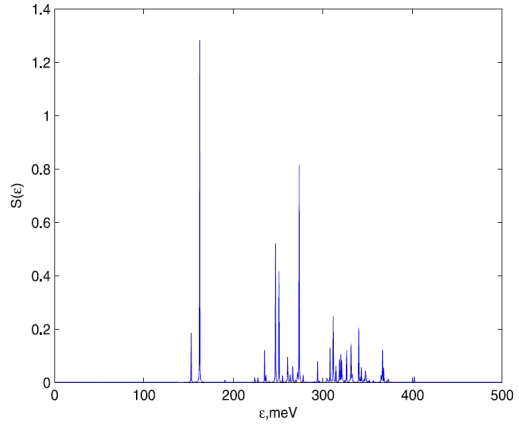

Fig. 9. Spin density of CoOEP within the THz region.

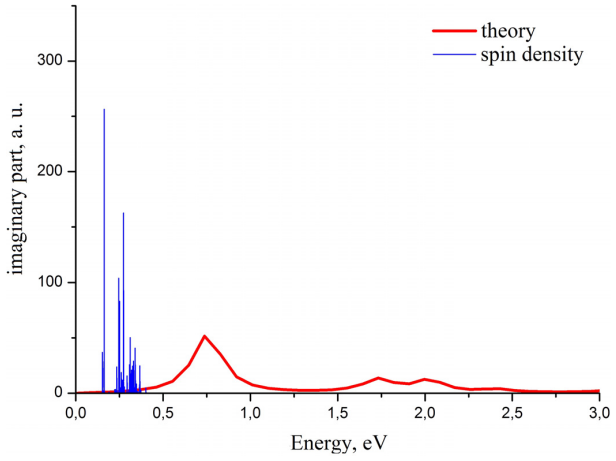

Fig. 10. (Color online) The comparison of the calculated spectra within the THz and visible regions.

The comparison of the spin density in the THz domain (see Fig. 9) and dielectric function in the visible region is presented in Fig. 10. The results show that the characteristic features of both spectra provide detailed information on the optical properties of CoOEP within both the terahertz and visible regions.

4. Conclusions

The obtained results provide an opportunity for a complex study of optical properties and spin structure of molecular cobalt octaethylporphyrin. The system under investigation shows the magnetic momentum of the central ions. The strength and sign of anisotropy and optical transparency within the visible and terahertz ranges are known to depend on the environment of the central metal atom (the ligand field). Consequently, these materials can be used as stable qubits and nanoelements for spintronics and quantum computing.

The optical properties, spin structure and spin dynamics of molecular magnets have been investigated. The theoretical spectra of the extinction coefficient, refraction index and absorption index have been calculated. These spectra provide valuable information about energy of optical transitions within the visible range. Moreover, to obtain the total energy range, the density of spin transitions within the terahertz range has been presented. The feature at 3.8 eV on the optical spectra seems to be caused by an interband optical transition, while several other detected features within the terahertz range could be the result of the spin crossover.

Acknowledgments

The authors would like to thank the Ministry of Education and Science of the Russian Federation for the financial support (Agreement No. 14.587.21.0002, Project Identifier RFMEFI 58714X0002).

References

1. W. M. Campbell, K. W. Jolley, P. Wagner, K. Wagner, P. J. Walsh, K. C. Gordon, L. Schmidt-Mende, M. K. Nazeeruddin, Q. Wang, M. Ratzel and D. L. Officer, *J. Phys. Chem. C* **111** (2007) 11760.
2. C. Yao, L. Yan, L. Guan, C. Liu, P. Song and Z. Su, *Dalton T.* **39** (2010) 7645.
3. S. Thyagarajan, T. Leiding, S. P. Årsköld, A. V. Cheprakov and S. A. Vinogradov, *Inorg. Chem.* **49** (2010) 9909.
4. S. M. Ribeiro, A. C. Serra and A. M. d'a Rocha Gonsalves, *J. Mol. Catal. A* **326** (2010) 121.
5. A. Verma, S. L. Facchina, D. J. Hirsch, S. Song, L. F. Dillahey, J. R. Williams and S. H. Snyder, *Mol. Med.* **4** (1998) 40.
6. J. S. Hu, H. X. Ji and L. J. Wan, *J. Phys. Chem. C* **113** (2009) 16259.
7. B. A. Friesen, B. Wiggins, J. L. McHale, U. Mazur and K. Hipps, *J. Am. Chem. Soc.* **132** (2010) 8554.
8. M. Momenteau and C. A. Reed, *Chem. Rev.* **94** (1994) 659.
9. B. Su, I. Hatay, A. Trojánek, Z. Samec, T. Khoury, C. P. Gros, J. M. Barbe, A. Daina, P. A. Carrupt and H. H. Girault, *J. Am. Chem. Soc.* **132** (2010) 2655.
10. S. Yamazaki, Y. Yamada, T. Ioroi, N. Fujiwara, Z. Siroma, K. Yasuda and Y. J. Miyazaki, *J. Electroanal. Chem.* **576** (2005) 253.
11. B. Steiger and F. C. Anson, *Inorg. Chem.* **39** (2000) 4579.
12. H. Z. Yu, J. S. Baskin, B. Steiger, F. C. Anson and A. H. Zewali, *J. Am. Chem. Soc.* **121** (1999) 484.
13. C. Joachim, J. Gimzewski and A. Aviram, *Nat.* **408** (2000) 541.
14. L. Bogani and W. Wernsdorfer, *Nat. Mater.* **7** (2008) 179.
15. S. Sanvito, *Chem. Soc. Rev.* **40** (2011) 3336.
16. M. Mannini, F. Pineider, P. Sainctavit, C. Danieli, E. Otero, C. Sciancalepore, A. M. Talarico, M.-A. Arrio, A. Cornia, D. Gatteschi and R. Sessoli, *Nat. Mater.* **8** (2009) 194.
17. Z. Xiong, D. Wu, Z. Valy Vardeny and J. Shi, *Nature* **427** (2004) 821.
18. A. J. Drew *et al.*, *Nat. Mater.* **8** (2009) 109.
19. P. Parida, A. Kundu and S. K. Pati, *Phys. Chem. Chem. Phys.* **12** (2010) 6924.
20. D. Ghosh, P. Parida and S. K. Pati, *J. Phys. Chem. C* **116** (2012) 18487.
21. D. Ghosh, P. Parida and S. K. Pati, *Appl. Phys. Lett.* **106** (2015) 193105.
22. P. Parida, S. K. Pati and A. Painelli, *Phys. Rev. B* **83** (2011) 165404.
23. C. Wäckerlin, K. Tarafder, D. Siewert, J. Girovsky, T. Haähle n, C. Iacovita, A. Kleibert, F. Nolting, T. A. Jung, P. M. Oppeneer and N. Ballav, *Chem. Sci.* **3** (2012) 3154.
24. W. Auwärter, D. Écija, F. Klappenberger and J. V. Barth, *Nat. Chem.* **7** (2015) 105.
25. H. Wende, M. Bernien, J. Luo, C. Sorg, N. Ponpandian, J. Kurde, J. Miguel, M. Piantek, X. Xu, Ph. Eckhold, W. Kuch, K. Baborschke, P. M. Ponchmatia, B. Sanyal, P. M. Oppeneer and O. Eriksson, *Nat. Mater.* **6** (2007) 516.
26. C. Wäckerlin, D. Chylarecka, A. Kleibert, K. Müller, C. Iacovita, F. Nolting, T. A. Jung and N. Ballav, *Nat. Commun.* **1** (2010) 61.
27. H. Kim, Y. H. Chang, S.-H. Lee, Y.-H. Kim and S.-J. Kahng, *ACS Nano* **7** (2013) 9312.
28. J. Girovsky, K. Tarafder, C. Wäckerlin, J. Nowakowski, D. Siewert, T. Hählen, A. Wäckerlin, A. Kleibert, N. Ballav, T. A. Jung and P. M. Oppeneer, *Phys. Rev. B* **90** (2014) 220404.
29. B. W. Heinrich, L. Braun, J. I. Pascual and K. J. Franke, *Nano Lett.* **15** (2015) 4024.
30. H. Kondo, J. Nara and T. Ohno, *J. Phys. Chem. C* **115** (2011) 6886.

31. F. Moresco, G. Meyer, K.-H. Rieder, H. Tang, A. Gourdon and C. Joachim, *Phys. Rev. Lett.* **86** (2001) 672.
32. W. J. Cho, Y. Cho, S. K. Min, W. Y. Kim and K. S. Kim, *J. Am. Chem. Soc.* **133** (2011) 9364.
33. V. A. Dediu, L. E. Hueso, I. Bergenti and C. Taliani, *Nat. Mater.* **8** (2009) 707.
34. T. Miyamachi, M. Gruber, V. Davesne, M. Bowen, S. Boukari, L. Joly, F. Scheurer, G. Rogez, T. K. Yamada, P. Ohresser, E. Beaurepaire and W. Wulfhekel, *Nat. Commun.* **3** (2012) 938.
35. C. Wäckerlin, K. Tarafder, J. Girovsky, J. Nowakowski, T. Hählen, A. Shchyrba, D. Siewert, A. Kleibert, F. Nolting, P. M. Oppeneer, T. A. Jung and N. Ballav, *Angew. Chem. Int. Edit.* **52** (2013) 4568.
36. G. Kresse and J. Hafner, *Phys. Rev. B* **47** (1993) 558(R).
37. J. P. Perdew, K. Burke and M. Ernzerhof, *Phys. Rev. Lett.* **77** (1996) 3865.
38. G. Kresse and D. Joubert, *Phys. Rev. B* **59** (1999) 1758.
39. H. J. Monkhorst and J. D. Pack, *Phys. Rev. B* **13** (1976) 5188.
40. L. Hedin, *Phys. Rev.* **139** (1965) A796.
41. M. S. Hybertsen and S. G. Louie, *Phys. Rev. B* **34** (1986) 5390.
42. O. Dubay, Visualization suite for VASP (2017), https://www.p4vasp.at.
43. OriginLab, Data analysis and graphing software (2017), http://www.originlab.com.
44. D. Loss and D. P. DiVincenzo, *Phys. Rev. A* **57** (1998) 120.